12-2009

Pressure Broadening and Shift of the Cesium D_1 Transition by the Noble Gases and N_2, H_2, HD, D_2, CH_4, C_2H_6, CF_4, and ^3He

Greg A. Pitz

Douglas E. Wertepny

Glen P. Perram
Air Force Institute of Technolgy

Recommended Citation

Pitz, G. A., Wertepny, D. E., & Perram, G. P. (2009). Pressure broadening and shift of the cesium D1 transition by the noble gases and N2, H2, HD, D2, CH4, C2H6, CF4, and 3He. Physical Review A, 80(6), 062718. https://doi.org/10.1103/PhysRevA.80.062718

Pressure broadening and shift of the cesium D_1 transition by the noble gases and N_2, H_2, HD, D_2, CH_4, C_2H_6, CF_4, and ^3He

Greg A. Pitz, Douglas E. Wertepny, and Glen P. Perram*
Department of Engineering Physics, The Air Force Institute of Technology, 2950 Hobson Way, Wright-Patterson Air Force Base, Ohio 45433-7765, USA
(Received 3 September 2009; published 21 December 2009)

The pressure broadening and shift rates for the cesium D_1 ($6\ ^2P_{1/2} \leftarrow 6\ ^2S_{1/2}$) transition with the noble gases and N_2, H_2, HD, D_2, CH_4, C_2H_6, CF_4, and ^3He were obtained for pressures less than 300 torr at temperatures under 65 °C by means of laser absorption spectroscopy. The collisional broadening rate, γ_L, for He, Ne, Ar, Kr, Xe, N_2, H_2, HD, D_2, CH_4, C_2H_6, CF_4, and ^3He are 24.13, 10.85, 18.31, 17.82, 19.74, 16.64, 20.81, 20.06, 18.04, 29.00, 26.70, 18.84, and 26.00 MHz/torr, respectively. The corresponding pressure-induced shift rates, δ, are 4.24, −1.60, −6.47, −5.46, −6.43, −7.76, 1.11, 0.47, 0.00, −9.28, −8.54, −6.06, and 6.01 MHz/torr. These rates have then been utilized to calculate Lennard-Jones potential coefficients to quantify the interatomic potential surfaces. The broadening cross section has also been shown to correlate with the polarizability of the collision partner.

DOI: 10.1103/PhysRevA.80.062718 PACS number(s): 34.50.−s, 32.70.Jz, 34.20.−b, 42.55.Xi

I. INTRODUCTION

The line shape, broadening, and shift of the atomic hyperfine profiles due to collisions with other atoms or molecules have been studied thoroughly and numerous reviews are available [1,2]. The alkali metals have been of recent interest as a lasing medium for diode pumped gas lasers. These alkali metal lasers were proposed by Krupke in 2003 and demonstrated by Beach in 2004, but this system may be considered an adaptation of a system first proposed by Schawlow and Townes in 1958 and built by Rabinowitz in 1962 [3–6]. This current effort will utilize large diode bars to pump the D_2 transition of the alkali metal and lase along the D_1 transition. This diode pumped alkali metal laser (DPAL) is a three level laser system that depends heavily on saturation of the pumped state; therefore, the linewidth matching of the D_2 transition with the diode bar or stack is crucial. Diode bars and stacks typically have a linewidth of 30 GHz which would force the cesium to be exposed to pressures up to 10 atm. The DPAL models are then dependent on the accuracy of the information on the collisional effects on the alkali metal. As part of a study to measure the spin-orbit energy transfer between the $6\ ^2P_{1/2}$ and $6\ ^2P_{3/2}$ states, the broadening and shift rates for the $6\ ^2P_{1/2} \leftarrow 6\ ^2S_{1/2}$ transition have been measured.

With the exception of two recent studies, the collisional effects on the cesium D_1 transition have not been updated since 1990 [7–9]. Andalkar utilized laser absorption spectroscopy in 2001 to study the effects of N_2 and He on Cs up to 160 Torr. Andalkar was able to achieve errors less then 1.2% [7,10]. In 2008, Couture *et al.* utilized a flash lamp and spectrometer to measure the shift and broadening rates of He, N_2, and ^{129}Xe with errors less than 3% [8]. One study in 1990, by Inoue, produced results with errors less than 1.6% [9]. The Inoue study utilized laser absorption spectroscopy and was limited not by the measurement of the widths of the spectrum but the measurements of the pressure, which had an error of 10%. The studies prior to 1990 produced results with errors around 20%, and most of these studies were performed at pressures less than 160 torr [11–15]. In addition to these experimental values for the collisional effects on cesium, Jacobson theoretically determined the values for broadening and shift rates for cesium with argon, krypton, and xenon from the interatomic potentials [16].

The rates that are currently available from these works vary greatly between each other. In the case of helium there is a discrepancy of 10 MHz/torr for the broadening rate and for nitrogen there is a 11 MHz/torr difference. Andalkar pointed this out in his study in 2001, but his study only included nitrogen and helium. This study provides updated rates for all the noble gases and H_2, HD, D_2, N_2, CH_4, C_2H_6, CF_4, and ^3He. Of which, HD, D_2, CH_4, C_2H_6, CF_4, and ^3He have never been measured. The lighter isotope of helium has been predicted from theory by Couture *et al.* using the ratio of reduced masses and the rate for ^4He. Also, no previous study witnessed any non-Voigt line shapes at low pressures and therefore did not determine if it has an effect on the collisional broadening and shift rates.

II. EXPERIMENT

This experiment utilized a Coherent MBR-110 Ti:sapphire ring laser tuned to 894 nm and scanned over 35 GHz. The ring laser, which was pumped by a Coherent Verdi V-18 diode laser, has a linewidth less than 100 kHz with a power less than 3.5 W. This beam was greatly attenuated (<1 μW) before reaching the test cell to avoid any saturation broadening and to stay within the Beer's law regime of absorption. The scan time was converted to the frequency utilizing an etalon with a free spectral range of 299.45 MHz, which was calibrated using the extremely well known hyperfine spacing of the D_1 line. The output of the ring laser was amplitude modulated, at a frequency of 1505 Hz, and coupled into a trifurcated fiber bundle. Each branch of the bundle was focused onto a different Hamamatsu silicon pho-

*glen.perram@afit.edu

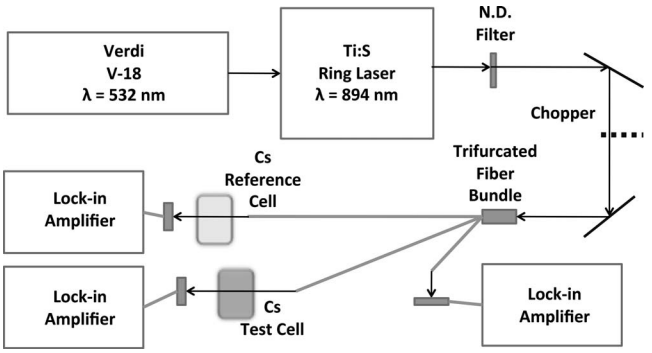

FIG. 1. Experimental apparatus for laser absorption spectroscopy.

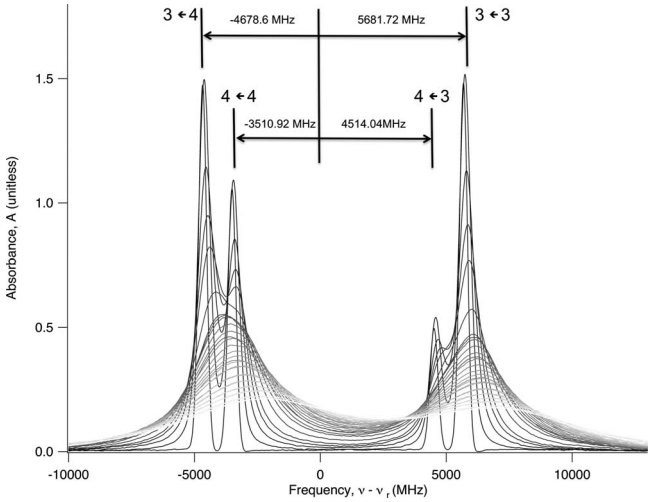

FIG. 2. The cesium D_1 hyperfine line-shape pressure broadened by ^{3}He from 10–300 Torr (in steps of 10 Torr) with the assigned $(F' \leftarrow F'')$ hyperfine transitions, where ν_r is line center for the D_1 transition.

todiode (model S2281-04). The photodiodes were employed to record the incident intensity on the cesium cells, a reference spectrum for an absolute frequency measurement via a low pressure cell, and the transmitting intensity of the test cell while observing the changing absorption profile.

Each cell was constructed from a 1-in.-long cylinder made of Pyrex glass with an ampoule of cesium attached underneath. The cells were affixed to the gas handling system with Ultratorr seals. This allowed for pressure measurements at the time of the scan while previously used prefilled cells only allowed for pressure measurement at the time it was filled, which created systematic error in addition to the pressure measurement error. The gas handling system also reduced the possibility of exposure to air and moisture, which would result in contamination of the cesium sample and could result in fire and creation of the very strong base, CsOH.

The cell was placed in a temperature controlled aluminum block with the ampoule exposed underneath. This configuration of the cesium ampoule and the oven was designed such that they could be controlled at two different temperatures allowing for better control of the number density of the cesium in the upper cell. The temperature controller maintained the temperature within 1 °C. The vapor pressure at the highest temperature (333 K) was 47.25 ± 3.86 μtorr [17]. The control of the temperature and number density was import to control the Doppler width and to avoid self-absorption issues at higher temperatures. Early on in the experimental process higher temperatures were used and this effect was seen in the relative amplitudes of the hyperfine spectrum at temperatures over 100 °C.

Cell pressure was monitored by MKS model 690A capacitance manometers with heads for 1000, 100, 10, and 1 Torr for cell pressures ranging from under 1 mTorr to 300 Torr. The cesium was 99.98% pure and all gases had a purity greater than 99.9% purity, with the one exception of HD which had a purity of 97.3%.

As shown in Fig. 1, phase sensitive detection was employed to monitor the transmitted laser intensities utilizing Stanford Research Systems lock-in amplifiers, model SR850. The recorded transmitted intensities, I, were ratioed with the incident intensity, I_0, which removed the low frequency power fluctuation from the laser. A small linear background was observed over the 35 GHz scan of the ring laser, which had a relatively small slope in comparison to its offset, 1.4×10^{-3}%. This was mathematically removed from the known absorption profile during the numerical fitting of the spectrum.

III. RESULTS

The hyperfine spectrum of the cesium D_1 transition is shown in Fig. 2, where the larger ground-state splitting (9.192 631 770 GHz) and the smaller $^2P_{1/2}$ state splitting (1.167 680 GHz) is observed [17]. In Fig. 2, the line-shape profile is shown at multiple pressures for ^{3}He and is a typical demonstration of all buffer gases and spectrums. Each spectrum, which has an average signal-to-noise ratio of 700, was collected over 3 min and consisted of over 100 000 data points. Each individual hyperfine component is observed at 0–100 torr and, as expected, becomes more convoluted as pressure increases but the larger ground-state hyperfine splitting is still evident at 300 torr. The hyperfine profile plays a significant role in the total line shape of the transition spectrum even at 1 atm [18]. In the sample spectra shown in Fig. 2, the ^{3}He spectra are slowly blueshifted, which is only observed for the lighter species studied which also includes, He, H_2, HD, and D_2.

The Lorentzian width and line center were determined from the absorption profile by a numerical fit of the spectrum to a set of four Voigt line shapes:

$$A = -Ln\left(\frac{I}{I_0}\right) = c_0 + c_1\nu + c_2\sum_{i=1}^{4} a_i V(\nu_i + \delta\nu, \Delta\nu_L; \gamma_D), \tag{1}$$

where $c_{0,1}$ are the coefficients for the linear background and c_2 is the absolute absorbance constant. The absorbance, A, is defined as $\sigma\, ln$, where σ is the cross section, l is the path length of the cell, and n is the number density. Each of the four hyperfine lines have been assumed to share the same

TABLE I. Cesium hyperfine transition strengths for the D_1 transition.

Transition	Strength
$S_{F\ F'}$	(Unitless)
$S_{4\ 4}$	5/12
$S_{4\ 3}$	7/12
$S_{3\ 4}$	3/4
$S_{3\ 3}$	1/4

Doppler, γ_D, and Lorentzian width, $\Delta\nu_L$. Both widths were measured as full width at half maximum values. The Doppler width was calculated via the formula

$$\gamma_D = 2\nu\sqrt{2\ \ln(2)\frac{k_b T}{mc^2}}, \tag{2}$$

where ν is the frequency, k_b is the Boltzmann constant, T is the temperature, m is the mass, and c is the speed of light. At the maximum temperature, 338 K, for this experiment the Doppler width is 384 MHz and the hyperfine line shape was constrained to have this calculated value of the Doppler width for its corresponding temperature. The hyperfine spectrum was also assumed to share a single spectral shift, $\delta\nu$, and each hyperfine line position, ν_i, is well known. A normalized Voigt profile, V, which utilized each of the known hyperfine line strengths, a_i, was employed. The line strengths are calculated from the product of the fractional Boltzmann population of the ground state and the transition strength, which are shown in Table I. The Voigt shape term was found to have a value of unity ($\Delta\nu_L = \gamma_D$) at a pressure of 20 torr with an average broadening rate of 20 MHz/torr.

Several fits of Eq. (1) to the observed spectra, with corresponding fit residuals, are provided in Fig. 3. The signal-to-noise is about 1500, allowing for an observation of the line shape well into the wings, with scan range of more than 130 Doppler widths. At pressures about 80 Torr, the average fit residuals are unstructured and about 10^{-5}%. For the lowest pressures ($P < 80$ Torr) a small systematic deviation from the Voigt profiles is observed. Allowing greater flexibility in the fitting of Eq. (1) by varying the Doppler width, relative Lorentzian widths of the hyperfine components or the hyperfine line strengths do not significantly reduce the structured residuals. Line narrowing due to velocity changing collisions was examined using several forms of the Gallatry profile [19,20]. While the qualitative features of the residuals are indeed matched, further analysis is required to fully characterize the rates for the velocity changing collisions. The effects of the small residuals at low pressures on the pressure broadening and the shift rates are negligible as discussed below. Prior studies of the O_2 A band exhibited line narrowing as well and also demonstrated the minor effects on the reported Lorentzian fit parameters [21].

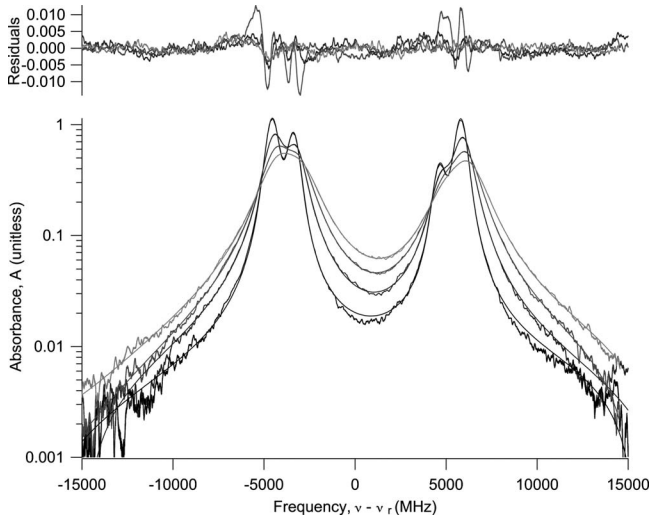

FIG. 3. A sample of the resultant fits with residuals to Eq. (1) for the D_1 transition under the influence of ^{3}He at 20, 40, 60, and 80 Torr.

The extracted shifts, $\delta\nu$, and Lorentzian width, $\Delta\nu_L$, are displayed as a function of pressure with various nonreactive collisional partners in Figs. 4 and 5. A linear fit of the data was performed and the extracted slopes are the shift and broadening rates. This corresponds to following formula for the Lorentzian width:

$$\Delta\nu_L = \gamma P + \gamma_N, \tag{3}$$

where γ is the broadening rate for the buffer gas, and γ_N is the natural width. The natural width is 4.575 MHz, which was calculated from the known lifetime of 34.791 ns. The natural linewidth was used for the y intercept and was fixed for the weighted linear fits that were performed on the data. Similarly, the shifts were fit to a line but with an intercept of 0 and the slope is the shift rate δ.

The resultant broadening and shift rates with their corresponding slope fit errors are shown in Table II as γ_1 and Table III as δ. The rates listed were determined from the fit of a line with a fixed y intercept. In other fits, the y intercepts were allowed to vary and on average varied 0.06 MHz/torr which is less than the average standard deviation. Also, the average y-intercept parameter was 2.25 MHz with an error of 9.89 MHz. The natural linewidth lies within the error bounds of the y-intercept parameter. Second, to determine the effect of the systematic residuals on the width and shift rates the points extracted from spectrum with this effect in the residuals were removed from the fit of Eq. (3). This produced on average no overall change in the slope of the line and all values for the broadening and shift rates were still well within the error bounds reported in Tables II and III.

The only other major contributing factor to the total error was from the pressure measurements, each of which had an error of 0.08%. The slope error was determined from a weighted fit of the data, where the weights were determined from the reciprocal of the Lorentzian width error. The error in the width and shifts was less than 0.34% on average.

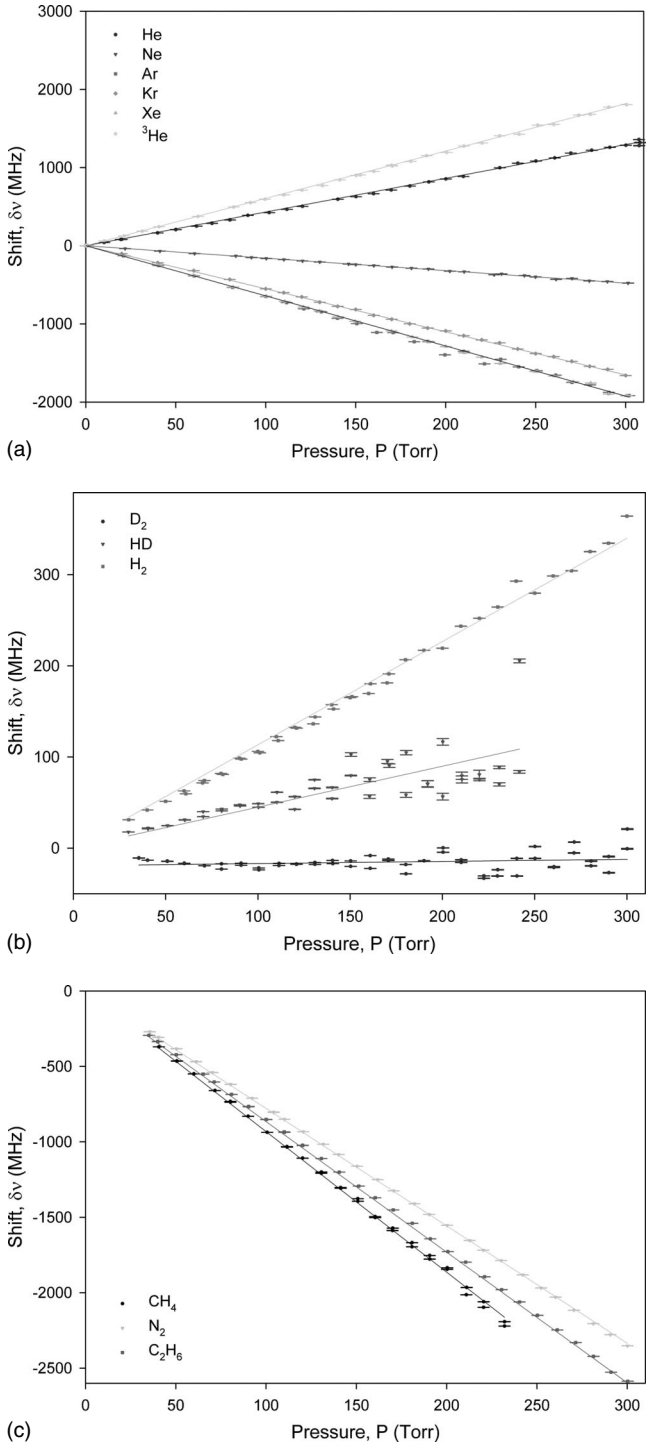

FIG. 4. D_1 hyperfine profile shift as a function of pressure of (a) the noble gases, (b) various hydrogen isotopes, and (c) several molecules.

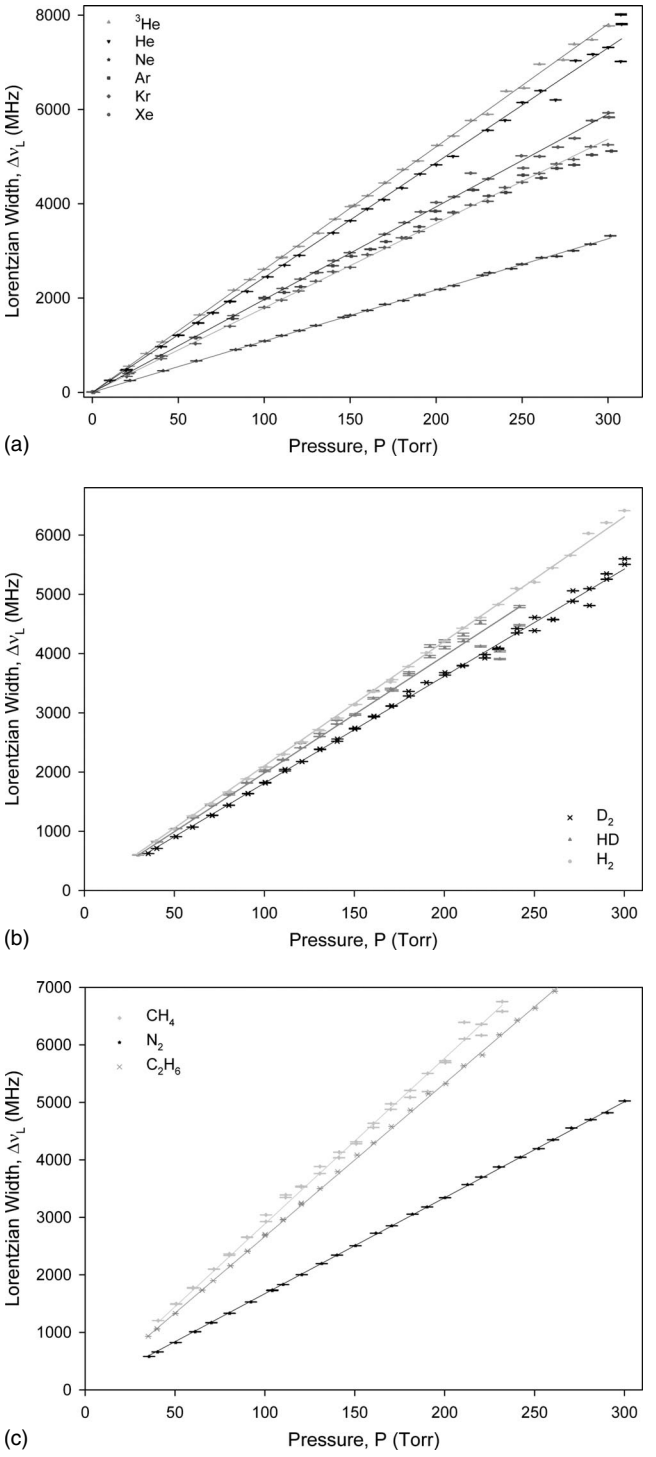

FIG. 5. D_1 hyperfine profile broadening as a function of pressure of (a) the noble gases, (b) various hydrogen isotopes, and (c) several molecules.

IV. DISCUSSION

In general, the present broadening rates are in approximate agreement with all but the earliest of the prior work. However, a detailed comparison requires an assessment of the temperature dependence. The broadening rates are certainly influenced by differences in the average relative speed, g, of the collision pairs, and may be further modified by an energy dependence to the cross section, σ:

$$\gamma = \int_0^\infty \sigma(g) g f(g;T) dg. \tag{4}$$

The temperature dependence of the Maxwellian speed distribution, $f(g;T)$, and the relative speed,

TABLE II. Measured values for the broadening rate for the D_1 transition compared to the previous results.

Current work			Previous work			
Buffer gas	T_1 (K)	γ_1 [a] (MHz/torr)	T_2 (K)	γ_2 (MHz/torr)	γ_{adj} [b] (MHz/torr)	Ref.
He	323	24.13 ± 0.07	294	26.21 ± 0.31	25.42	[7]
			295	19.49 ± 1.35	18.62	[13]
			393	28.42 ± 1.03	31.34	[8]
^{3}He	323	26.00 ± 0.05	393	21.71 ± 0.70 [c]	23.94	[8]
Ne	313	10.85 ± 0.02	295	10.13 ± 0.86	9.75	[13]
Ar	313	18.31 ± 0.16	295	19.64 ± 0.23	19.06	[13]
			295	14.99[d]	14.55	[16]
Kr	313	17.82 ± 0.05	295	19.84 ± 2.5	19.26	[12]
			295	15.29[d]	14.84	[16]
Xe	313	19.74 ± 0.08	295	21.49 ± 2.60	20.86	[12]
			295	17.09[d]	16.59	[16]
H_2	328	20.81 ± 0.09	295	40.42 ± 6.20	39.24	[12]
HD	318	20.06 ± 0.12				
D_2	318	18.04 ± 0.04				
N_2	318	15.82 ± 0.05	294	19.51 ± 0.06	19.07	[7]
	323	16.36 ± 0.02	295	30.93 ± 5.71	29.33	[13]
	333	15.66 ± 0.08	393	14.73 ± 0.69	16.00	[8]
CH_4	333	29.00 ± 0.10				
C_2H_6	331	26.70 ± 0.03				
CF_4	318	18.84 ± 0.05				

[a]Error from a weighted linear fit only.
[b]See Eq. (6).
[c]Calculated value from ^{4}He.
[d]Calculated from theoretical interatomic potentials.

$$g = \sqrt{8k_bT/\pi\mu}, \tag{5}$$

where μ is the reduced mass of the collision pair, leads to a temperature dependence of the broadening rate often described as [22]

$$\gamma_2(T_2) = \gamma_1(T_1)\left(\frac{T_1}{T_2}\right)^n. \tag{6}$$

Note that the collision rates are dependent on concentration and the pressure is related to the concentration via another temperature factor, $P=nk_BT$. If the cross section is independent of speed, $\gamma=g\sigma$ and $n=1/2$. Table II provides the previously reported broadening rates, γ_2, scaled to the current temperatures for comparison as γ_{adj}. A test of the energy independence of the cross section is best afforded by the current temperature dependence of the nitrogen data provided in Fig. 6.

The shift rates are also in agreement with the previous studies, but a direct comparison is difficult with current data. These rates can be calculated from the cross section and the velocity distribution, but in the case of the shifts, the cross section may have a more significant energy dependence. So, the assumption used for the broadening rate comparison cannot be made and, thus, the value of $n \neq 1/2$. Couture *et al.* attempted to determine the value of n for his rates utilizing both his and Andalkar's data [8]. Couture *et al.* calculated the value for He to be 1.6 ± 0.5, while this current study has shown that the value for n in the Cs-N_2 interactions is approximately 1/2. With such a limited amount of data and large error bounds, further study is needed.

Equations (4) and (5) have been utilized by Couture *et al.* to show a means for calculating the rates for similar atoms with slight differences in mass, as is the case for ^{4}He and ^{3}He. This mass dependence arises from the relative speeds in Eq. (5) and can be expressed as

$$\gamma_2(T_2) = \gamma_1(T_1)\left(\frac{\mu_2}{\mu_1}\right)^{1/2}. \tag{7}$$

Employing this expression Couture *et al.* calculated the value within 1.7 MHz/torr of the value obtained in the laboratory. This difference may again be explained by an energy dependence within the cross section which may depend on the individual atomic potentials.

TABLE III. Measured values for the shift rates for the D_1 transition compared to the previous results.

	Current work		Previous work		
Buffer gas	T_1 (K)	δ [a] (MHz/torr)	T_2 (K)	δ (MHz/torr)	Ref.
He	323	4.24 ± 0.02	294	4.46 ± 0.03	[7]
			295	6.61 ± 1.00	[13]
			393	$4.45 \pm .69$	[8]
^{3}He	323	6.01 ± 0.01	393	5.82 ± 1.03 [b]	[8]
Ne	313	-1.60 ± 0.01	295	-2.88 ± 0.09	[13]
Ar	313	-6.47 ± 0.03	295	-8.73 ± 0.4	[13]
			295	-5.4 [c]	[16]
Kr	313	-5.46 ± 0.01	295	-2.65 ± 0.10	[13]
			295	-5.4 [c]	[16]
Xe	313	-6.43 ± 0.01	295	-8.09 ± 1.2	[13]
			295	-6.3 [c]	[16]
H_2	328	1.11 ± 0.01	295	2.25 ± 0.19	[13]
HD	318	0.47 ± 0.03			
D_2	318	$0.0009 \pm 0.000\ 04$			
N_2	318	-7.69 ± 0.01	294	-8.23 ± 0.02	[7]
	323	-7.71 ± 0.01	295	-7.38 ± 0.11	[13]
	333	-7.41 ± 0.01	393	-8.90 ± 0.69	[8]
CH_4	333	-9.28 ± 0.02			
C_2H_6	331	-8.54 ± 0.01			
CF_4	318	-6.06 ± 0.01			

[a]Error from a weighted linear fit only.
[b]Calculated value from ^{4}He.
[c]Calculated from theoretical interatomic potentials.

From the rates themselves the interatomic potentials can be calculated. These potentials can be determined by using the ratio of the broadening and shift rates and the impact approximation [23]. Assuming the potentials have a Lennard-Jones form,

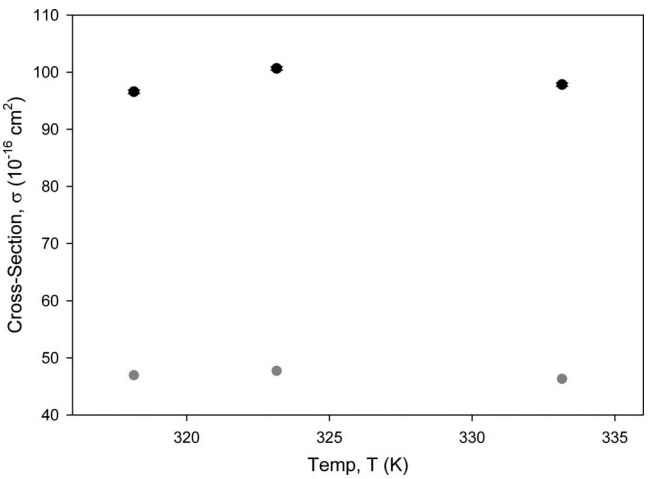

FIG. 6. The cross section for broadening (●) and shift (○) of Cs-N_2 interaction at three different temperatures.

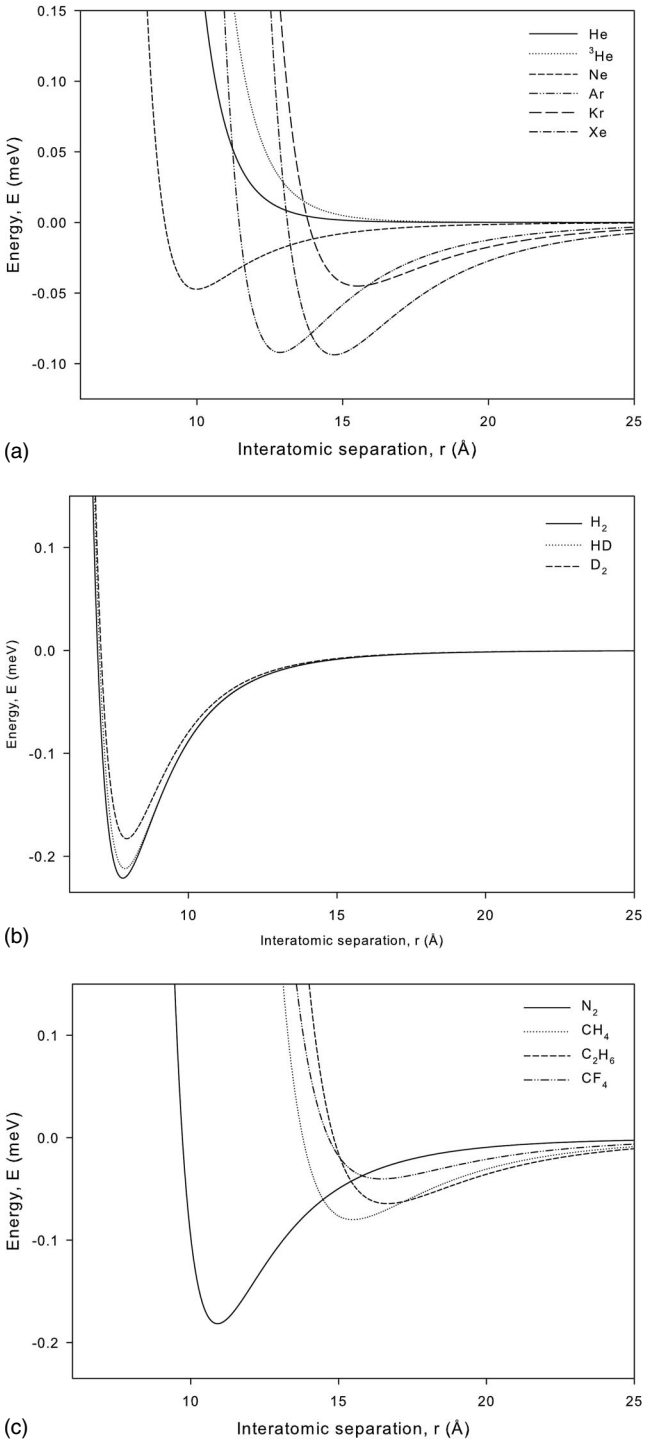

FIG. 7. Calculated interatomic potentials for (a) the noble gases, (b) various forms of hydrogen, and (c) an assortment of molecules.

$$V(R) = C_{12}r^{-12} - C_6r^{-6}, \tag{8}$$

where R is the interatomic separation and C_6 and C_{12} are the coefficients for the R^{-6} and R^{-12} parts of the potential, respectively. The broadening and shift rates have been analyzed before utilizing this approach [2]. The potentials derived from this work are shown in Fig. 7. These curves compare closely to those of Rotondaro's work with rubidium

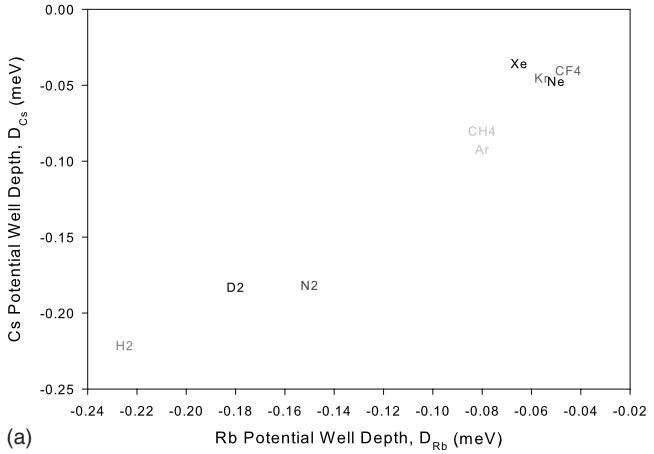

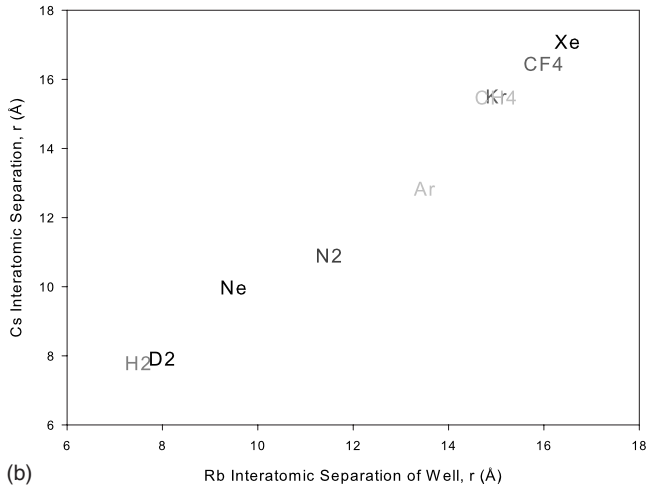

FIG. 8. Comparison between the well depths (a) and the interatomic separation (b) of cesium and rubidium.

[24]. This comparison is shown in Fig. 8, with similar interatomic distances and binding energies. Yet, this model has ignored the effects of rotational degrees of freedom, nonspherically symmetric potentials, spin-orbit energy transfers, and any curved trajectories.

The impact approximation and the Lennard-Jones potential suggest a linear correlation between the probability per collision for phase changing collisions and polarizability. The present results are consistent with this prediction as illustrated in Fig. 9. The ratio for the gas kinetic cross section,

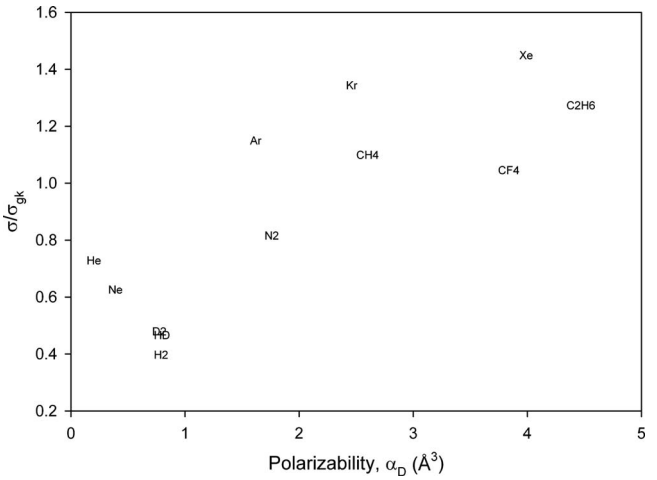

FIG. 9. Correlation of the probability for phase changing collisions in the D_1 transition with dipole polarizability of the collision partner.

$$\sigma_g = \pi(r_{\mathrm{Cs}} + r_{buffer\ gas})^2, \tag{9}$$

was evaluated from Ref. [25]. The polarizability for the buffer gases was found in Ref. [26].

V. CONCLUSIONS

The reported rates for collision-induced line broadening and shifts for the cesium D_1 line with errors of about 0.3% enable enhanced accuracy in modeling the performance of diode pumped alkali metal lasers. Conversion of the observed rates to the interatomic potential unifies the results for a wide range of buffer gases and enables the comparison to another heavy alkali metal, Rb. The effects of the line narrowing are observed at low pressures; further analysis is needed to discern the role of velocity changing collisions.

ACKNOWLEDGMENTS

Support for this work from the Air Force Office of Scientific Research and the High Energy Laser Joint Technology Office is gratefully acknowledged. We want to thank M. D. Rotondaro for his help with the rubidium potentials.

[1] N. Allard and J. Kielkopf, Rev. Mod. Phys. **54**, 1103 (1982).
[2] W. R. Hindmarsh and J. M. Farr, Prog. Quantum Electron. **2**, 141 (1973).
[3] W. F. Krupke, R. J. Beach, V. K. Kanz, and S. A. Payne, Opt. Lett. **28**, 2336 (2003).
[4] R. J. Beach, J. Opt. Soc. Am. B **21**, 2151 (2004).
[5] A. L. Schawlow and C. H. Townes, Phys. Rev. **112**, 1940 (1958).
[6] P. Rabinowitz, Appl. Opt. **1**, 513 (1962).
[7] A. Andalkar and R. B. Warrington, Phys. Rev. A **65**, 032708 (2002).
[8] A. H. Couture, T. Clegg, and B. Drieguys, J. Appl. Phys. **104**, 094912 (2008).
[9] Y. Inoue, K. Uchida, H. Hori, and T. Sakurai, J. Phys. Soc. Jpn. **59**, 516 (1990).
[10] A. Andalkar, Ph.D. thesis, University of Washington, 2001.
[11] R. O. Garrett and S. Y. Ch'en, Phys. Rev. **144**, 66 (1966).
[12] E. Bernabeu, J. Opt. Soc. Am. **67**, 24 (1977).
[13] E. Bernabeu and J. M. Alvarez, Phys. Rev. A **22**, 2690 (1980).
[14] Z. Siegling, Z. Naturforsch. Teil A **39A**, 447 (1984).

[15] S. L. Izotova, N. I. Kaliteevskii, G. F. Lekhto, and M. S. Frish, Opt. Spectrosc. **59**, 293 (1985).
[16] H. Jacobson, Phys. Rev. A **4**, 1363 (1971).
[17] D. A. Steck, http://steck.us/alkalidata
[18] G. Pitz and G. Perram, in *SPIE Proceedings of the Tenth International Symposium on Gas Flow and Chemical Lasers*, edited by C. R. Phipps (SPIE, Bellingham, WA, 2008), Vol. 7005.
[19] R. H. Dicke, Phys. Rev. **89**, 472 (1953).
[20] L. Galatry, Phys. Rev. **122**, 1218 (1961).
[21] K. J. Ritter and T. Wilkerson, J. Mol. Spectrosc. **121**, 1 (1987).
[22] J. F. Kielkopf, J. Phys. B **9**, L547 (1976).
[23] J. H. Sanders, *Progress in Quantum Electronics* (Pergamon Press, New York, 1973).
[24] M. D. Rotondaro, J. Quant. Spectrosc. Radiat. Transf. **57**, 497 (1997).
[25] J. O. Hirschfelder, C. F. Curtiss, and R. B. Bird, *Molecular Theory of Gases and Liquids* (Wiley, New York, 1954).
[26] H. L. Anderson, *A Physicist's Desk Reference* (American Institute of Physics, New York, 1989).